Effect of Upstream ULF Waves on the Energetic Ion Diffusion at the Earth's Foreshock. II. Observations

Arpad Kis[1], Shuichi Matsukiyo[2], Fumiko Otsuka[2], Tohru Hada[2], Istvan Lemperger[1],
Iannis Dandouras[3], Veronika Barta[1], and Gabor Facsko[1,4]

[1] Research Centre for Astronomy and Earth Sciences, Geodetic and Geophysical Institute, 9400 Sopron, Csatkai u. 6-8, Hungary
akis@ggki.hu, Kis.Arpad@csfk.mta.hu
[2] Faculty of Engineering Sciences, Kyushu University, Kasuga, Fukuoka, Japan
[3] IRAP, University of Toulouse/UPS/CNRS/CNES, 9 Av. Colonel Roche, BP 44346, F-31028 Toulouse cedex 4, France

Abstract

This study reports observations of energetic ions upstream of the Earth's quasi-parallel bow shock by *Cluster* at times when interspacecraft separation distances were large. We analyze two individual upstream ion events during high solar wind velocity conditions to compare the spatial evolution of partial energetic ion densities in front of the Earth's bow shock along the magnetic field line. Using a bow shock model, we determine the distance of SC1 and SC3 to the bow shock surface parallel to the magnetic field. The CIS-HIA instrument on board *Cluster* provides partial energetic ion densities in four energy channels between 10 and 32 keV. Using the differences of the partial energetic ion densities observed on SC1 and SC3, and the distances of the spacecraft to the bow shock, we determine the spatial gradient of partial energetic ion densities at various distances from the bow shock. We show, for the first time, that the e-folding distance and the diffusion coefficient of the diffuse ions become unusually small when these ions interact with high-intensity waves generated by a strong field-aligned beam.

Key words: acceleration of particles – diffusion – plasmas – shock waves – waves

1. Introduction

Energetic ions with energies from slightly above solar wind energy up to a few hundred keV upstream of the Earth's bow shock have been subject to detailed investigation since their early reports by Asbridge et al. (1968) and by Lin et al. (1974). Studies showed that these energetic ions have two different sources, so they can be divided into energetic ions of magnetospheric origins (Sarris & Krimigis 1988; Posner et al. 2002) and bow shock related ions. Bow shock related ions are those that have been reflected and/or accelerated by the Earth's bow shock (Gosling et al. 1989). According to the angle Θ_{Bn}, between the shock normal and the upstream magnetic field direction, shocks are classified as quasi-perpendicular ($\Theta_{\mathrm{Bn}} > 45°$) or quasi-parallel ($\Theta_{\mathrm{Bn}} < 45°$). Typically, ions associated to the quasi-perpendicular side of the Earth's bow shock exhibit characteristics of a more beam-like distribution in velocity space streaming away from the bow shock and moving against the incoming solar wind along the upstream magnetic field lines (Paschmann et al. 1980). On the other hand, the velocity distribution of energetic ions in front of a quasi-parallel bow shock, the so-called diffuse ions, exhibits an isotropic characteristic with a shock-directed bulk velocity that is slower than the solar wind (Scholer et al. 1981). Paschmann et al. (1979) reported a third kind of energetic ion group forming a distribution with intermediate characteristics between a beam-like and an isotropic distribution. Kis et al. (2007) showed that the beam-like distribution of the so-called field-aligned beams (FAB) ions can evolve first into an intermediate and later into a toroidally gyrating ion distribution. The toroidally gyrating ions can be found deeper in the foreshock region as a consequence of an interaction with self-induced waves and convection by the solar wind. Originally, it

was proposed that the ions forming the FAB might provide the principal seed population for the diffusive ion acceleration mechanism. Ipavich et al. (1984) demonstrated that the He/H ratio of energetic ions at about 30 keV in the upstream region is highly correlated with He/H ratio in the solar wind. At the same time, the He/H density ratio in the FAB is dramatically smaller than that measured simultaneously in the solar wind (see Ipavich et al. 1988 and Fuselier & Thomsen 1992). These results indicate that the solar wind ions, and not the FAB ions, are the primary source for the diffuse ions. The diffuse ions in front of the quasi-parallel bow shock are always observed in the presence of hydromagnetic waves (Hoppe et al. 1981). This realization has led to a broadly accepted concept of an intense interplay between waves and energetic ions in the foreshock region. The waves are thought to be scattering centers for the energetic ions, resulting in pitch-angle scattering without changing the energy of the ions. Energetic ions are also known to excite waves in front of the Earth's quasi-parallel bow shock. Hoppe et al. (1981) demonstrated that energetic ions are accompanied in this region by large-amplitude waves of their own making in the 0.01–0.3 Hz frequency range. These waves are mostly transversal waves. An overview on waves and their generation mechanisms upstream of quasi-parallel collisionless shocks can be found in Wilson (2016). The coupling between diffuse ions and waves (i.e., the generation of waves by diffuse ions) was described by Lee (1982, 1983) in a self-consistent model. One essential element of this model is the direct coupling between the energetic particle density and the wave energy density in the frequency range that is resonant with the energetic particles. Möbius et al. (1987) found a good agreement between the predicted and the measured wave energy density when analyzing two upstream ion events. Trattner et al. (1994) extended this study by analyzing more than 300 upstream energetic ion events and found a remarkably high correlation of 0.89 between the predicted and the observed

wave energy density. They also point out that the correlation describes the local coupling between the wave and the energetic ion energy; i.e., the correlation is independent of the strength of an event and its position relative to the shock. The study by Kennel et al. (1986) showed that the predicted wave power spectral density agrees very well with observations also in the case of an interplanetary traveling shock. Gordon et al. (1999) presented a revised and more generalized version of the self-consistent theory of ion diffusive shock acceleration and the associated generation of waves. To conclude, the waves in front of the quasi-parallel bow shock are produced locally by diffuse ions, and the wave energy density grows linearly with the energized ion energy density. This also means that under normal interplanetary conditions, the diffuse ions are scattered by these self-induced waves. The consequence of pitch-angle scattering is spatial diffusion that ultimately leads to first order Fermi acceleration of these ions at the bow shock (Axford et al. 1977; Scholer 1985). The theory of steady state diffusive shock acceleration predicts that the density of energetic ions (with energy E) falls off exponentially from the shock front into the upstream region. The e-folding distance, is given by the relation $L(E) = K(E)/v_{sw}$, where $L(E)$ is the e-folding distance, $K(E)$ is the diffusion coefficient at E ion energy and v_{sw} is the solar wind bulk velocity. Here, we assume that the solar wind bulk velocity direction, the magnetic field, and the shock normal are aligned (see Axford et al. 1977). The same e-folding distance results in a steady state when ions diffuse from a source against the solar wind convection (Parker 1965). To prove that the behavior of diffuse ions indeed can be described by the diffusive transport theory, it is crucial to determine how the diffuse ion density spatial decrease along the magnetic field. Early attempts to describe the spatial variation of the upstream energetic ion distribution used single spacecraft data; therefore, they had to be done on a statistical basis. The necessity of a statistical study can be understood easily by taking into consideration the high variability of the solar wind conditions. Ipavich et al. (1981) analyzed 33 upstream particle events and demonstrated that the differential proton flux density at ~33 keV decreased exponentially with an e-folding distance of $L = 7 \pm 2\,R_E$ upstream of the Earth's bow shock. They calculated the distance from the bow shock only in the radial direction (i.e., roughly along the bow shock normal) and used an average bow shock model to obtain the bow shock location (Fairfield 1971). A crucial step in understanding diffusive shock acceleration and the pitch-angle scattering of energetic ions in front of the Earth's quasi-parallel bow shock was the study by Trattner et al. (1994), who completed a statistical analysis of about 300 upstream energetic ion events. In their study, the shock position was derived from the solar wind ram pressure and the distance from the spacecraft to the shock was determined along the interplanetary magnetic field. The results showed that the e-folding distance increases with energy and varies from $3.2 \pm 0.2\,R_E$ at 10 keV to $9.3 \pm 1\,R_E$ at 67 keV. These statistical studies show the importance of diffusive transport and acceleration in the upstream region. Observations prove that these upstream events can vary largely in intensity from event to event. Therefore, a statistical analysis can lead to a significant uncertainty of the determined e-folding distances. The *Cluster* mission allowed, for the first time, for the determination of the spatial gradient of diffuse ions during individual events. Using simultaneous data from at least two spacecraft provides the possibility of separating the spatial

variations of the plasma parameters from the temporal ones. This method result in a higher accuracy of the e-folding distance of the partial energetic ion density in the foreshock region. The work by Kis et al. (2004) was the first attempt to determine the e-folding distance of diffuse ions in the 10–32 keV ion energy range using simultaneous multispacecraft data of a single upstream ion event. The derived e-folding distance was about half of the value obtained previously on a statistical basis by Ipavich et al. (1981) and by Trattner et al. (1994). Kronberg et al. (2009) extended the analysis of that particular upstream event to the 30–160 keV energy range. Trattner et al. (2013) determined an unusually large e-folding distance value for protons with >14 keV energy in front the Earth's bow shock. That study was based on data provided by the IBEX Background Monitor. However, in their work, they also mentioned that the obtained e-folding distance cannot be directly compared to earlier measurements, since the instrument observes only a fraction of the total upstream ion distribution.

2. Observations

For this study, we use data provided by the *Cluster* spacecraft (SC). The upstream ion events were chosen by taking into consideration three conditions that need to be satisfied at the same time. These conditions are

1. the SC needs to be in the solar wind for a longer time period and positioned at large distance (i.e., more than 6–7 R_E) from the bow shock surface,
2. the SC configuration needs to have a large interspacecraft separation distance, and
3. the SC need to observe diffuse ions for longer time periods at various distances from the bow shock.

The purpose of this study is to offer observational evidence for the contribution of the FAB-generated waves on the scattering process of diffuse ions in front of the Earth's quasi-parallel bow shock. Therefore, we have chosen one upstream ion event when there was a strong FAB and another one when we could not detect any FAB.

Kis et al. (2007) and Kis et al. (2004) analyzed the upstream ion event observed by *Cluster* on 2003 February 18. On this occasion, a strong FAB was recorded as the SC were on the inbound leg of their orbit. The second work discusses the scattering of this FAB in the vicinity of the upstream boundary of the foreshock region on the quasi-parallel side of the Earth's bow shock. Since this is the only upstream ion event in the *Cluster* database fulfilling the previously mentioned three conditions and with the presence of a strong FAB, we have chosen this event for our investigation. As second event for this investigation, we have chosen an upstream ion event when the general conditions were similar compared to the first case. This is the upstream event on 2003 February 4. These two events are close in time (only two weeks separate them); therefore, the orbit—which is a polar orbit fixed in the interstellar coordinate system—is also similar. In both cases, we have a high solar wind speed, high Mach number case: on the February 4, the average solar wind bulk velocity was $\sim585\ \mathrm{km\,s^{-1}}$; while on February 18, the spacecraft recorded a solar wind bulk velocity of $\sim626\ \mathrm{km\,s^{-1}}$. During both events, the *Cluster* SC were moving toward the bow shock, i.e., they were on the inbound leg of their orbit. The ion data used in this study was provided by the *Cluster* Ion Spectrometer (CIS), which consists of the Hot Ion Analyzer (HIA) and the Composition and Function

analyzer (CODIF). The description of the instrument can be found in Rème et al. (2001). HIA uses a top hat electrostatic analyzer with no species discrimination. We have chosen the HIA for this study because CIS-HIA has a better energy resolution above 10 keV than CODIF. The HIA provides measurements of partial upstream ion densities in the following energy ranges: 10–13 keV, 13–18 keV, 18–24 keV, and 18–32 keV. We exclusively use data recorded on board SC1 and SC3 due to technical reasons (there is no CIS data available from SC2, and we do not obtain HIA data from SC4). The *Cluster* Flux Gate Magnetometer (FGM; Balogh et al. 2001) provides the magnetic data. Another similarity between the two cases is that SC1 was situated for the whole time period under investigation closer to the bow shock, while SC3 was farther out in the upstream direction. The distance between the two spacecraft was changing from about 1.5 R_E to about 1 R_E as the spacecraft were moving toward the bow shock. The distance between the spacecraft was large enough to record a statistically significant difference in the partial energetic ion density at the two spacecrafts' locations, and it is suitable to determine accurately the energetic ion partial density gradient. To determine the density gradient of diffuse ions in front of the Earth's quasi-parallel bow shock, first we need to find the spacecraft distance to the bow shock along the magnetic field. Subsequently, we need to calculate the difference of diffuse ion partial densities between the two spacecraft. The latter procedure has to be repeated for all four energy ranges available in the 10–32 keV energy range. To calculate the distance of the spacecraft to the bow shock, we used the bow shock model of Peredo et al. (1995). This model provides a (normalized) bow shock surface for a given Mach number in 3D. Horbury et al. (2001) demonstrated that the bow shock normals given by this model agree well with the normal directions determined by in situ measurements. The model was scaled to the real (i.e., observed) bow shock crossing that can be determined directly from *Cluster* data. Next, we modified the scaling as a function of the variations in the solar wind pressure for the time period prior the bow shock crossings. This semi-empiric, dynamic bow shock model provides us the distance of SC1 and SC3 to the bow shock along the magnetic field line with high precision. This is done by taking into consideration the exact place of the bow shock crossing and the changing of the stand-off distance due to variations in the solar wind pressure. According to our results, this dynamically scaled bow shock model is more accurate than other models that use only the solar wind and interplanetary magnetic field parameters. This method also provides the value of θ_{Bn}, i.e., the angle between the local magnetic field and the bow shock surface normal at the magnetic field–bow shock intersection point. Figures 1 and 2 present the ion energy spectrum recorded by SC1 versus the time for the two cases. As it can be seen, in both cases one can observe energetic ions above 10 keV energy, which show the presence of diffuse ions. This means that the spacecraft are in the foreshock region, i.e. the spacecraft are magnetically connected to the quasi-parallel side of the shock. The spacecraft crosses the bow shock at around 11:37 UT on February 4 and around 22:40 UT on February 18 and moves down into the magnestosheath. While on February 18, the spacecraft can be seen to record a continuous diffuse ion presence for the time period under investigation in the other case (February 4), the connection to the quasi-parallel bow shock is intermittent. In both figures, the horizontal red bar(s)

between the two panels show(s) the time period that was used to determine the diffuse ion gradient. The green bars in the bottom panel mark those time periods when the magnetic field power was generated (see Figure 4).

Figure 3 presents the evolution of the SC distance to the bow shock along the magnetic field line (top panels) and the value of θ_{Bn} (bottom panels) versus time for the February 4 and for the February 18 upstream ion events. Each symbol represents one measurement or data point. During the February 4 event, the connection to the quasi-parallel bow shock surface was intermittent. When the SC are connected to the quasi-parallel side of the bow shock, the value of θ_{Bn} decreases (with most of the time significantly below 45°). Note that there are time periods when the θ_{Bn} values are missing; during these times, the SC were not connected to the bow shock surface at all. Note that only those distances presented in the top panel were used in the determination of the diffuse ion gradient. All other data points were removed. In contrast, during the February 18 event (right), the connection to the quasi-parallel bow shock was almost continuous. In this case, the value of θ_{Bn} most of the time remains far below 45°. Closer to the bow shock, the direction of the local magnetic field sometimes changes to quasi-perpendicular. This effect is due to the presence of large-amplitude magnetic structures in the close vicinity of the bow shock.

Figure 4 presents the time evolution of the magnetic field wave power as the spacecraft moves closer to the bow shock during February 4 and 18, respectively. For these plots, we used high-resolution magnetic data (i.e., 5 Hz) provided by the FGM instrument. The panels present the magnetic field power versus frequency in a log–log scale. In both cases, the distance to the bow shock decreases from left to right; the left panels present the magnetic field power away from the shock, while the right ones present the power in the close vicinity of the bow shock; the middle ones present the intensity of magnetic wave power at middle distance from the bow shock. To produce the magnetic field power at various distances from the bow shock, we have carefully selected 12-minute time periods during which the SC was connected continuously to the quasi-parallel bow shock (i.e., there was a continuous presence of diffuse ions). Ion spectra and magnetic field data have been carefully checked to ensure that magnetic structures like short large-amplitude magnetic structures (SLAMS), long pulsations (LPs), or other transient phenomena were excluded. During the February 4 event, we witness a continuous (almost linear) increase of the wave power versus time in the 0.01–0.1 Hz frequency range. Since the plots are in a log–log scale, this corresponds to an exponential increase in wave power as the distance to the bow shock decreases. On the other hand, during the February 18 case, one can observe an intense, high peak in power in the 0.01–0.1 Hz frequency range even at large distances from the bow shock. This peak is continuously present with slightly changing intensities as the spacecraft moves closer to the bow shock. Note that the peak intensity is almost two orders of magnitude higher compared to the intensity of the wave power recorded at the February 4 event. (The reason for this considerable difference in wave power between the two cases—and the consequences—will be discussed in the following section.) It is equally noteworthy that close to the bow shock, the difference in the power between the two cases becomes less significant.

Figures 5 and 6 present the ion distributions in velocity space observed at the February 4 and 18 events. These distributions
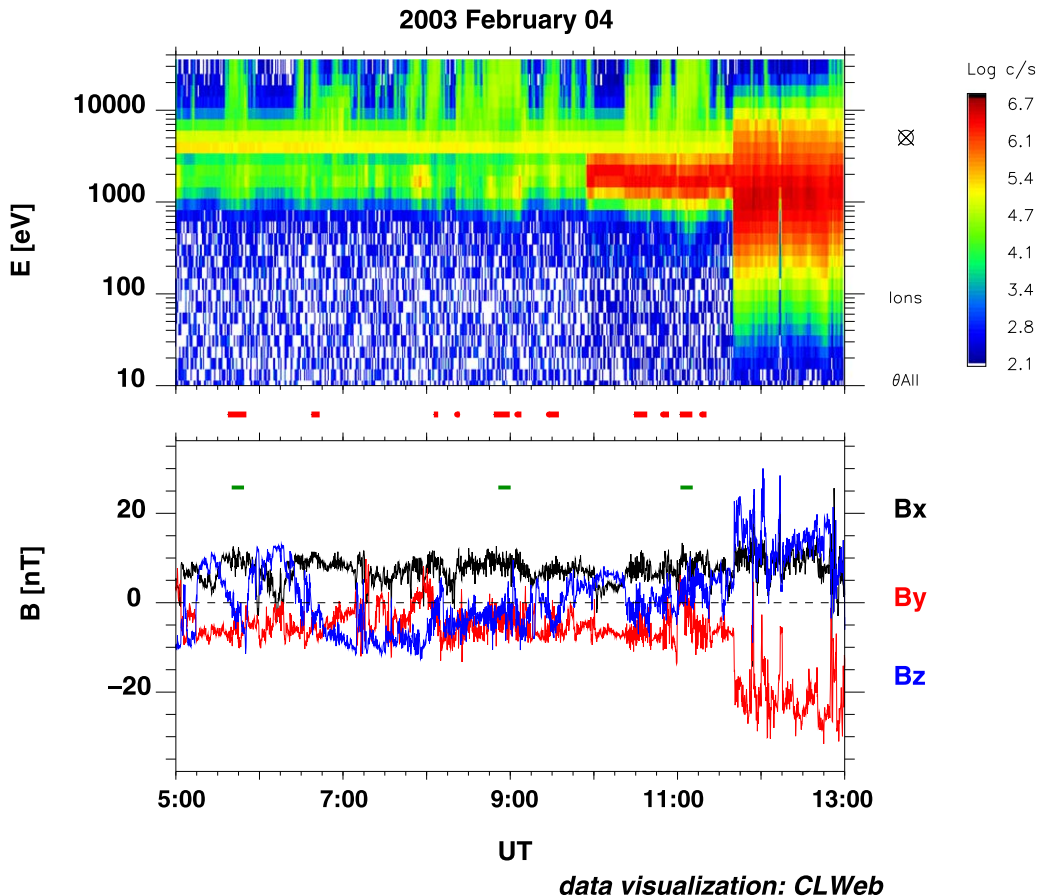
2003 February 04

Figure 1. Ion energy spectrum (top panel) and the magnetic field components in geocentric solar ecliptic (GSE) coordinates (bottom panel) vs. the time recorded by SC1 during the 2003 February 4 upstream ion event. The ion energy spectrum exhibits a presence of energetic/diffuse ions above 10 keV. The SC is situated in the foreshock region on magnetic field lines connected to the quasi-parallel bow shock. The connection to the quasi-parallel side of the bow shock is intermittent. The spacecraft crosses the bow shock at around 11:37 UT and moves into the magnetosheath. The horizontal red bars between the two panels show the time periods that were used to determine the diffuse ion gradient. The horizontal green bars in the bottom panel mark those time periods when the magnetic power was produced (see Figure 4).

show the ion distribution for the same time period that was also used to produce the magnetic wave power (see Figure 4). There is one exception: in Figure 6, one distribution (the one at 12:22 UT) presents the FAB distribution that was observed directly by the *Cluster* SC. This distribution has a completely other characteristic compared with the other distributions; it presents a highly anisotropic distribution that contains the solar wind and a strong FAB. Note that the FAB propagates along the magnetic field and is directed opposite to the solar wind flow.

To determine the energetic ion gradient, we carefully analyzed the ion data and used only those time periods when diffuse ions were present; all other time periods were omitted from the study. Of course, this applies only to the February 4 case. In both cases, we obtained hundreds of gradient values at various distances from the bow shock. To provide the same conditions of analysis for both cases, we used only the gradient values that were obtained at distances between 1 and 6 R_E to the shock along the magnetic field line. This protocol was used to prevent the contamination of ion data by the closeness of the shock and to exclude the possibility of other effects that might influence the scattering of energetic ions at larger distances from the bow shock.

The spatial gradient of the partial ion density was calculated in the four energy bands available in the 10–32 keV range. The spatial gradient was obtained using the difference of the partial ion density at the two spacecraft (SC1 and SC3) and the

difference of the spacecraft distances to the bow shock along the magnetic field. The gradient values than were attributed to the average distance of the two spacecraft to the bow shock surface along the magnetic field. Finally, the data set was reorganized as a function of distance to the bow shock.

3. Discussion

In diffusion against convection, the partial ion densities are known to fall off exponentially as a function of distance from the shock in the upstream region. Therefore, the gradient values were plotted versus distance in a lin-log scale. The gradient points in this representation (i.e., in a linear-logarithmic scale) can be fitted by a straight line, which provides us the e-folding distance along the magnetic field line. This has been done in the case of each upstream ion event at the four highest ion energy levels/bands available. Figure 7 presents the e-folding distance versus ion energy for both events.

In both cases, the e-folding distances are seen to increase as a function of ion energy, which is expected from the theory and is in harmony with previous observations. On the other hand, the e-folding distance values at every energy range differ significantly at the two events: the e-folding distances are considerably larger at the February 4 event when compared to the e-folding distance values obtained at the February 18 event. This demonstrates that the scattering is much more
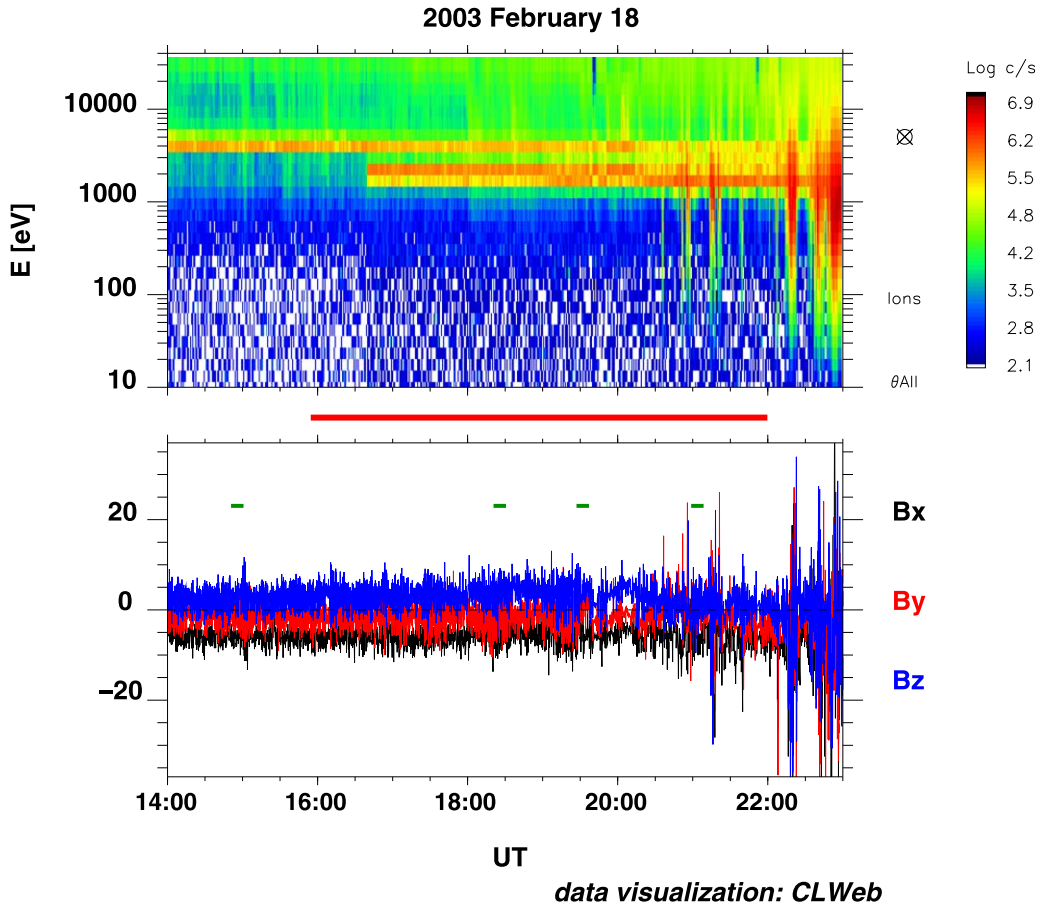
Figure 2. SC1 ion spectra and magnetic field observations during the 2003 February 18 event in a format similar that of Figure 1. The SC were continuously connected to the quasi-parallel bow shock, and during the whole interval, an intensive wave activity typical of the foreshock region can be observed. The spacecraft crossed the bow shock near 22:40 UT. The horizontal red bar between the two panels indicates the time period that was used to determine the diffuse ion gradient. The green bars in the bottom panel mark those time periods when the magnetic power was produced (see Figure 4).
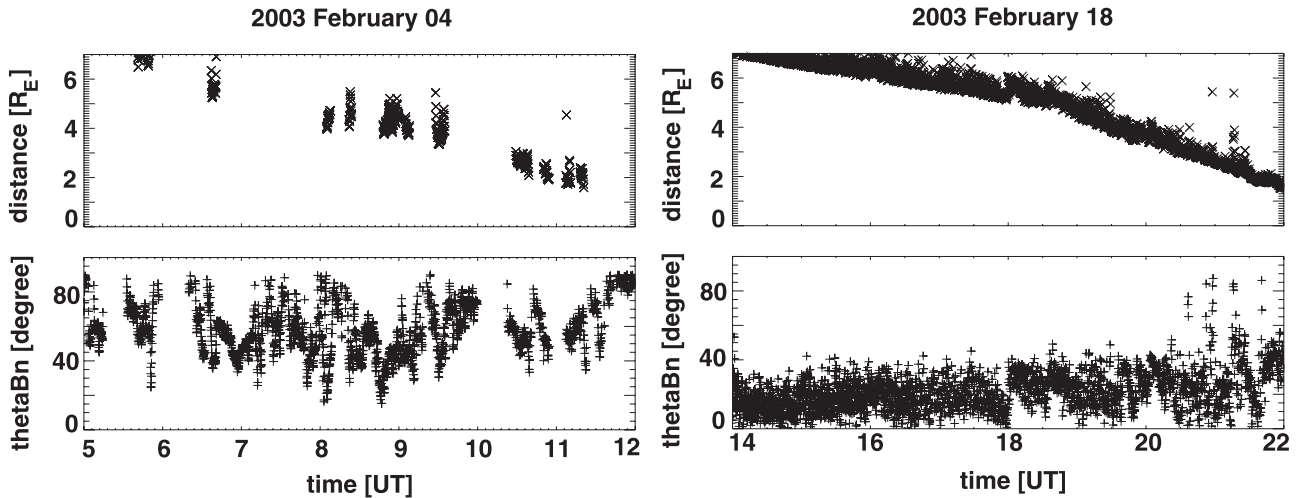
Figure 3. Distance of SC to the bow shock along the magnetic field line (top panels) and the value of θ_{Bn} (bottom panels) vs. time for the February 4 (left side) and for the February 18 cases (right side). Each symbol (the "x" symbol for distance and the cross symbol for the θ_{Bn}) represents one measurement/data point. During the February 4 event, the connection to the quasi-parallel bow shock surface is intermittent. When the SC is connected to the quasi-parallel side of the bow shock, the value of θ_{Bn} is seen to decrease, most of the time significantly below 45°. Note that there are time periods when the θ_{Bn} values are missing; during these time periods, the SC were not connected magnetically to the bow shock surface at all. Also note that only those distances are presented in the top panel, which was used in the determination of the diffuse ion gradient. All other data points were removed. During the February 18 event, the connection to the quasi-parallel bow shock was practically continuous. For this case, the value of θ_{Bn} remained for most of the time below 45°.

efficient in the latter case. To explain this difference, we need to compare the magnetic wave power recorded in the two cases. Figure 4 reveals that in the February 4 case, as the

spacecraft moves closer to the shock, there is a constant increase in wave power. The work by Lee (1982, 1983) describes the theoretical model of the wave generation by
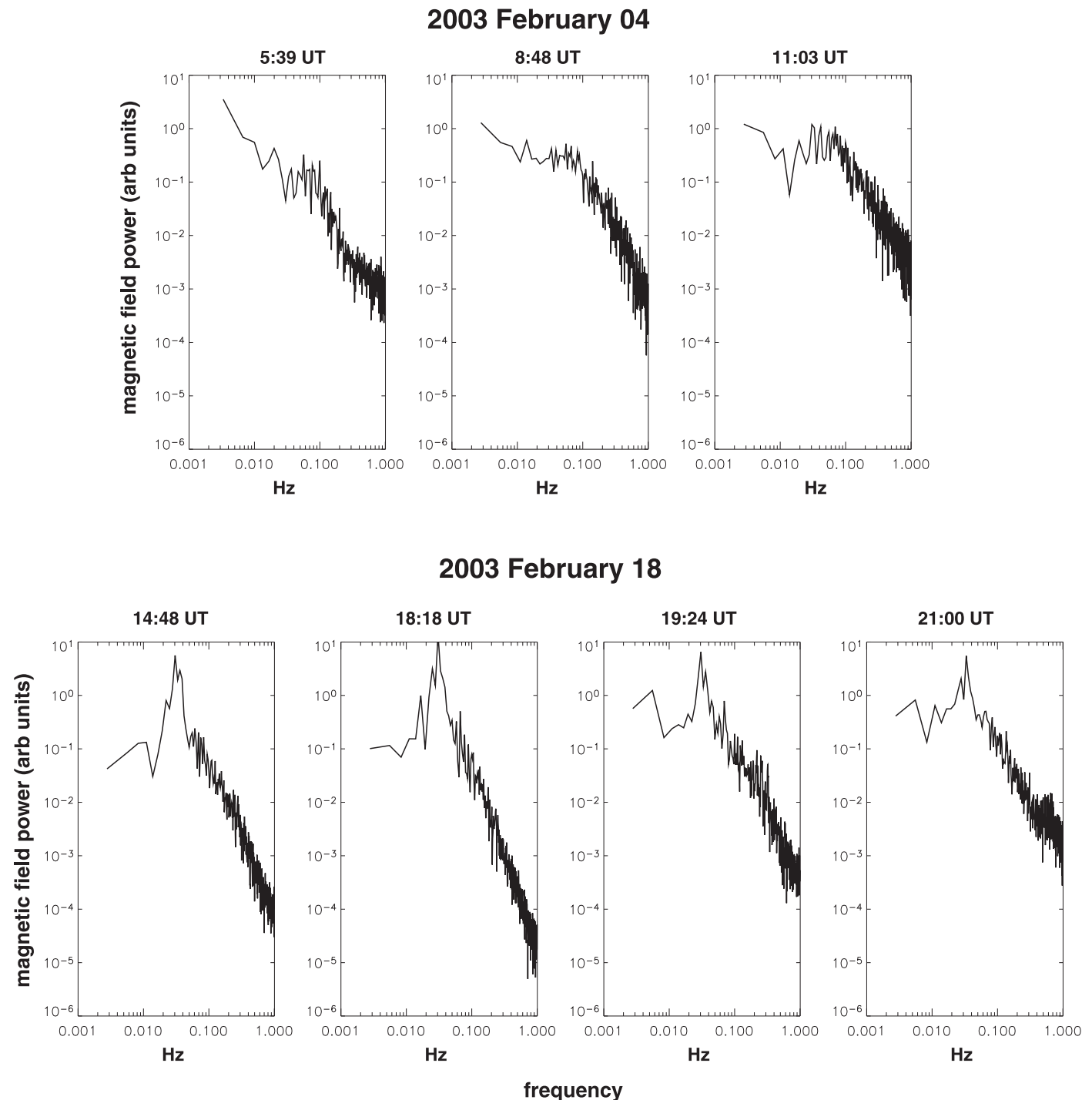
2003 February 04

2003 February 18

frequency

Figure 4. Time evolution of magnetic power density as the spacecraft moves closer to the bow shock during the February 4 (top panels) and the February 18 (bottom panels) event. Each plot shows high-resolution magnetic data (i.e., 5Hz) provided by the FGM instrument on board *Cluster*. The panels present the magnetic power vs. frequency in the log–log scale. The top panels present (from left to right) the magnetic power at 5:39, 8:48, and 11:03 UT (on February 4), which correspond to distances of about 6–7 R_E , 4–5 R_E, and 2 R_E to the bow shock along the magnetic field line, respectively. As shown, when the SC moves closer to the bow shock, there is a significant increase in the wave power density in the 0.01–0.1 Hz range, which broadly corresponds to the resonance frequency of the diffuse ions. The bottom panels (from left to right) present the power recorded at 14:48, 18:18, 19:24, and 21:00 UT (on February 18), which correspond to distances of about 7 R_E, 5 R_E, 3.5 R_E, and 2 R_E to the bow shock along the magnetic field lines, respectively. There is a persistent high peak in the magnetic power density with a virtually constant intensity all the way to the bow shock. Note that the peak intensity is about one or two orders of magnitude higher than the largest wave intensity recorded during the February 4 event.

diffuse ions. One important conclusion of this model is that the energetic particle density is directly proportional to the wave energy density in the resonant frequency range with the energetic ions. In other words, as the partial density of diffuse ions grows exponentially when moving closer to the

shock, the wave intensity (that is reflected in wave power) is also expected to grow exponentially.

This is the well-known, ordinary case of the diffusive shock acceleration (DSA) mechanism. The February 4 case presents all the features of this mechanism: the wave power grows as the
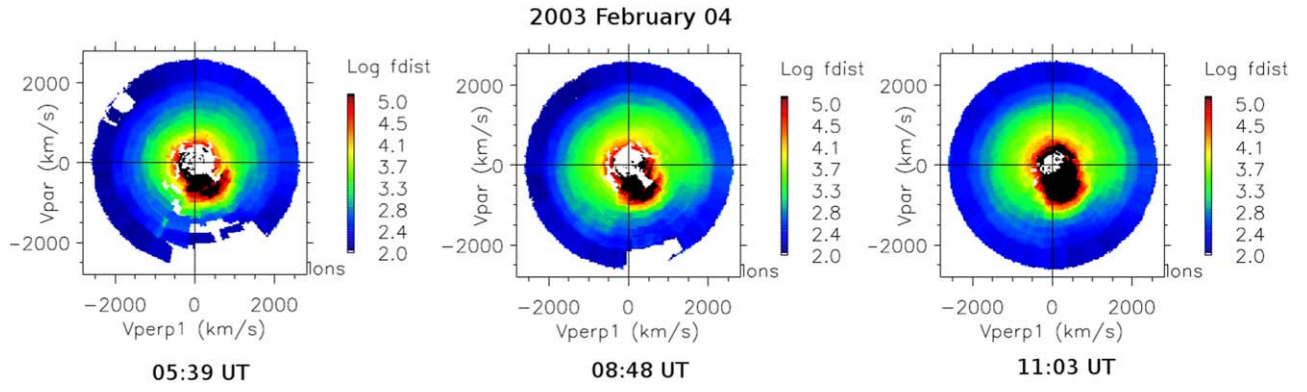
Figure 5. Ion distribution functions at the 2003 February 4 event in the velocity space in v_parallel vs. $v_\mathrm{perpendicular}$ coordinates. The distributions (from left to right) were taken at 05:39, 08:48, and 11:03 UT, respectively. These times are the same when the magnetic field was produced (see Figure 4). Each distribution is an isotropic, diffuse ion distribution.
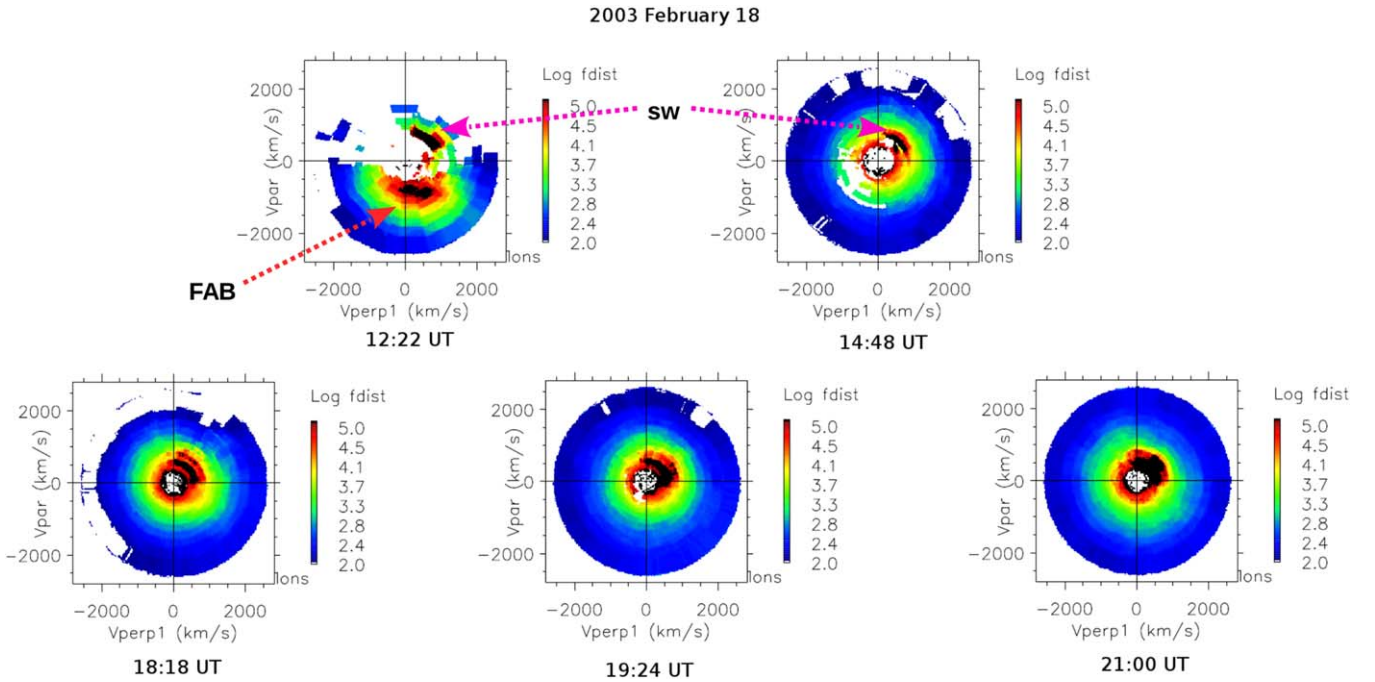

Figure 6. Ion distribution functions at the February 18 event in velocity space in v_parallel vs. $v_\mathrm{perpendicular}$ coordinates. The distributions were taken at 12:22, 14:48, 18:18, 19:24, and 21:00 UT, respectively. The panels present highly isotropic diffuse ion distributions at 14:48, 18:18, 19:24, and 21:00 UT; these are the same times when the magnetic power was produced. The distribution at 12:22 UT has different characteristics compared with the other distributions; it presents a highly anisotropic distribution that contains the solar wind beam and a strong FAB. Note that the FAB propagates along the magnetic field and in an opposite direction from the solar wind.

diffuse ion density grows. In the February 18 case, the magnetic wave power exhibits a completely different behavior, as it can be seen in Figure 4; the wave power has a high peak that is persistently present as the spacecraft moves closer to the bow shock. Since the diffuse ion density grows in a similar way to that of the February 4 case, we can confirm that the peak in the wave power cannot be produced by the diffuse ions and, therefore, must come from another source. Kis et al. (2007) discuss the presence of this peak in the wave power and reach the conclusion that the waves exhibiting the peak are generated by the FAB located in the upstream direction, at a larger distance from the bow shock. Therefore, we can conclude that in the February 18 case, we have two different wave sources: the waves that are generated locally by the diffuse ions and other waves that are produced far upstream, which are convected by the solar wind deep into the foreshock region. The evolution

of the wave power as a function of distance from the bow shock, in this case, suggests that these two wave groups are overlapping in the foreshock region and are scattering the diffuse ions together. This leads to a significantly smaller e-folding distance that can be observed in Figure 7.

Obviously, the value of the e-folding distance alone does not provide exact information about the efficiency of the scattering of diffuse ions and about the DSA mechanism. In order to compare the two upstream events in a proper way, we need to determine the parallel diffusion coefficient. We calculate the diffusion coefficient along the magnetic field using the e-folding distance values and by taking into consideration the solar wind velocity and direction and the angle between the solar wind and the magnetic field direction. According to the DSA theory, the diffusion coefficients should be similar to or just under normal conditions. Figure 8 presents the parallel
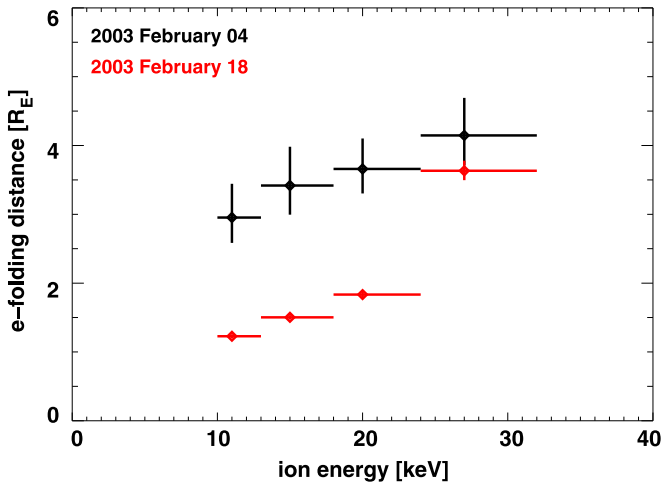
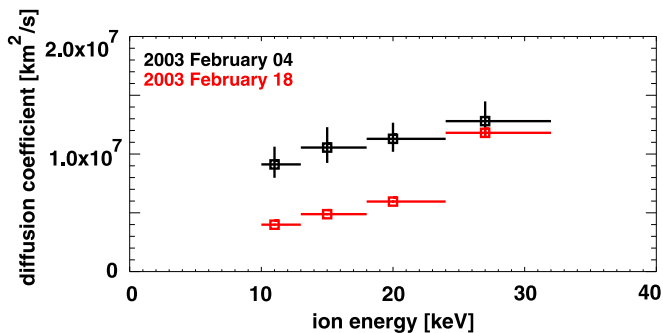**Figure 7.** Presentation of the e-folding distances determined for the 2003 February 4 (in black) and February 18 (in red) upstream ion events vs. ion energy. The horizontal bar shows the energy range (i.e., ion energy resolution) covered by the HIA instrument, while the vertical bar shows the error of the e-folding distance value. The e-folding distance values are significantly smaller during the February 18 upstream ion event (especially at bottom ion energies) when the SC recorded the peak in the magnetic field power density (see Figure 4).

Figure 8. Diffusion coefficient values for the 2003 February 4 (in black) and the February 18 (in red) upstream ion events vs. ion energy. The horizontal bar shows the energy range (i.e., ion energy resolution) covered by the HIA instrument, while the vertical bar shows the error of the diffusion coefficient. In the 10–24 keV energy range, the diffusion coefficient values obtained at the February 18 event are less than half of the value that were obtained at the February 4 event. In the 24–32 keV energy range, the difference between the two cases is not so striking, but there is still a visible difference between them.

diffusion coefficients versus energy at the two upstream ion events. The diffusion coefficient values are seen to differ significantly in all ion energies during the two upstream ion events. In bottom ion energies (i.e., between 10–24 keV), the diffusion coefficient of the February 4 event is more than twice as large as the diffusion coefficient determined using the data of the February 18 event. The difference is not as considerable in 24–32 keV ion energy range, but it is still noticeable. A difference of this magnitude cannot be explained by an eventual difference in θ_{Bn} value between the two cases. Figure 9 presents the position and shape of the bow shock and its relation to the FAB and the magnetic field direction at the 2003 February 18 event. It can be seen that during the whole time of the investigation the SC are situated downstream of the FAB.

It is important to mention that the ratio of the parallel diffusion coefficients in the two cases (i.e., with and without a wave field that is generated by a FAB) agrees very well with the simulation results presented in Otsuka et al. (2018).
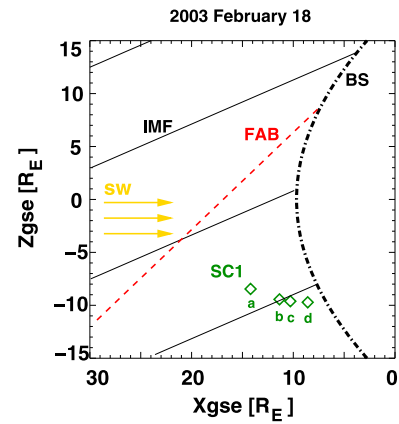

Figure 9. Position and shape of the bow shock and its relation to the FAB and the magnetic field direction at the 2003 February 18 event in Z_{GSE} vs X_{GSE} coordinates. The green diamonds show the SC position at 14:48, 18:18, 19:24, and 21:00 UT (from a to d, respectively). During the whole time period, the *Cluster* SC are seen to be situated at about 10–20 R_E distance downstream of the FAB. This distance is slightly modulated by the changing in the interplanetary magnetic field (IMF) direction.

4. Summary and Conclusions

In this study, we analyzed two upstream ion events during practically identical solar wind velocity conditions. The analysis shows that the e-folding distances of the diffuse ions in the 10–32 keV energy range can vary substantially from event to event. The diffusion coefficients of diffuse ions also differ significantly. These results suggest that this difference is due to the waves generated by the FAB that originate at the quasi-perpendicular side of the bow shock during one of the upstream events. This shows that occasionally a stronger than usual FAB can be formed that is capable of exciting high-intensity waves as it propagates in the upstream direction. These waves are convected deep into the foreshock region. If these waves have a higher intensity compared to the waves that are self-consistently produced by the bow shock accelerated diffuse ions, they can significantly influence the scattering process of the diffuse ions, resulting in a more intensive scattering. The effect obviously leads to an enhanced diffusive acceleration, which is a mechanism that is suggested for the first time. How often the diffusive acceleration at the quasi-parallel bow shock is influenced by waves that are produced by an FAB remains an unresolved question. We should like to note that, for the first time, we have demonstrated the simultaneous global interaction between processes at the quasi-perpendicular and at the quasi-parallel sides of the Earth's bow shock.

ORCID iDs

Fumiko Otsuka ⓘ https://orcid.org/0000-0002-7190-7799

References

Asbridge, J. R., Bame, S. J., & Strong, I. B. 1968, JGR, 73, 5777
Axford, W. I., Leer, E., & Skadron, G. 1977, Proc. ICRC, 11, 132
Balogh, A., Carr, C. M., Acuña, M. H., et al. 2001, AnGeo, 19, 1207
Fairfield, D. H. 1971, JGR, 76, 6700
Fuselier, S. A., & Thomsen, M. F. 1992, GeoRL, 19, 437
Gordon, B. E., Lee, M. A., Möbius, E., & Trattner, K. J. 1999, JGR, 104, 28263
Gosling, J. T., Thomsen, M. F., Bame, S. J., & Russell, C. T. 1989, JGR, 94, 3555
Hoppe, M. M., Russell, C. T., Frank, L. A., Eastman, T. E., & Greenstadt, E. W. 1981, JGR, 86, 4471
Horbury, T. S., Cargill, P. J., Lucek, E. A., et al. 2001, AnGeo, 19, 1399
Ipavich, F. M., Galvin, A. B., Gloeckler, G., Scholer, M., & Hovestadt, D. 1981, JGR, 86, 4337
Ipavich, F. M., Gloeckler, G., Hamilton, D. C., Kistler, L. M., & Gosling, J. T. 1988, GeoRL, 15, 1153
Ipavich, F. M., Gosling, J. T., & Scholer, M. 1984, JGR, 89, 1501
Kennel, C. F., Coroniti, F. V., Scarf, F. L., et al. 1986, JGR, 91, 11917
Kis, A., Scholer, M., Klecker, B., et al. 2004, GeoRL, 31, L20801
Kis, A., Scholer, M., Klecker, B., et al. 2007, AnGeo, 25, 785
Kronberg, E. A., Kis, A., Klecker, B., Daly, P. W., & Lucek, E. A. 2009, JGR, 114, A03211
Lee, M. A. 1982, JGR, 87, 5063
Lee, M. A. 1983, JGR, 88, 6109
Lin, R. P., Meng, C.-I., & Anderson, K. A. 1974, JGR, 79, 489
Möbius, E., Scholer, M., Sckopke, N., et al. 1987, GeoRL, 14, 681
Otsuka, F., Matsukiyo, S., Kis, A., Nakanishi, K., & Hada, T. 2018, ApJ, 853, 117
Parker, E. N. 1965, P&SS, 13, 9
Paschmann, G., Sckopke, N., Asbridge, J. R., Bame, S. J., & Gosling, J. T. 1980, JGR, 85, 4689
Paschmann, G., Sckopke, N., Bame, S. J., et al. 1979, GeoRL, 6, 209
Peredo, M., Slavin, J. A., Mazur, E., & Curtis, S. A. 1995, JGR, 100, 7907
Posner, A., Schwadron, N. A., Zurbuchen, T. H., et al. 2002, GeoRL, 29, 1099
Rème, H., Aoustin, C., Bosqued, J. M., et al. 2001, AnGeo, 19, 1303
Sarris, E. T., & Krimigis, S. M. 1988, GeoRL, 15, 233
Scholer, M. 1985, GMS, 35, 287
Scholer, M., Hovestadt, D., Ipavich, F. M., & Gloeckler, G. 1981, JGZG, 49, 186
Trattner, K. J., Allegrini, F., Dayeh, M. A., et al. 2013, JGRA, 118, 4425
Trattner, K. J., Mobius, E., Scholer, M., et al. 1994, JGR, 99, 13389
Wilson, L. B. 2016, GMS, 216, 269